Dual-Responsive Glycopolymers for Intracellular Co-Delivery of Antigen and Lipophilic Adjuvants

Judith De Mel¹, Mehjabeen Hossain³, Oluwaseyi Shofolawe-Bakare², Sk Arif Mohammad¹, Emily Rasmussen³, Khadeeja Milloy¹, Micaela Shields¹, Eric W. Roth⁵, Karan Arora⁶, Rafael Cueto⁷, Shou-Ching Tang⁴, John T. Wilson⁶, Adam E. Smith^{1, 2}, Thomas A. Werfel¹⁻⁴

¹Department of Biomedical Engineering, University of Mississippi, University, MS, USA, 38677

²Department of Chemical Engineering, University of Mississippi, University, MS, USA, 38677

³Department of BioMolecular Sciences, University of Mississippi, University, MS, USA, 38677

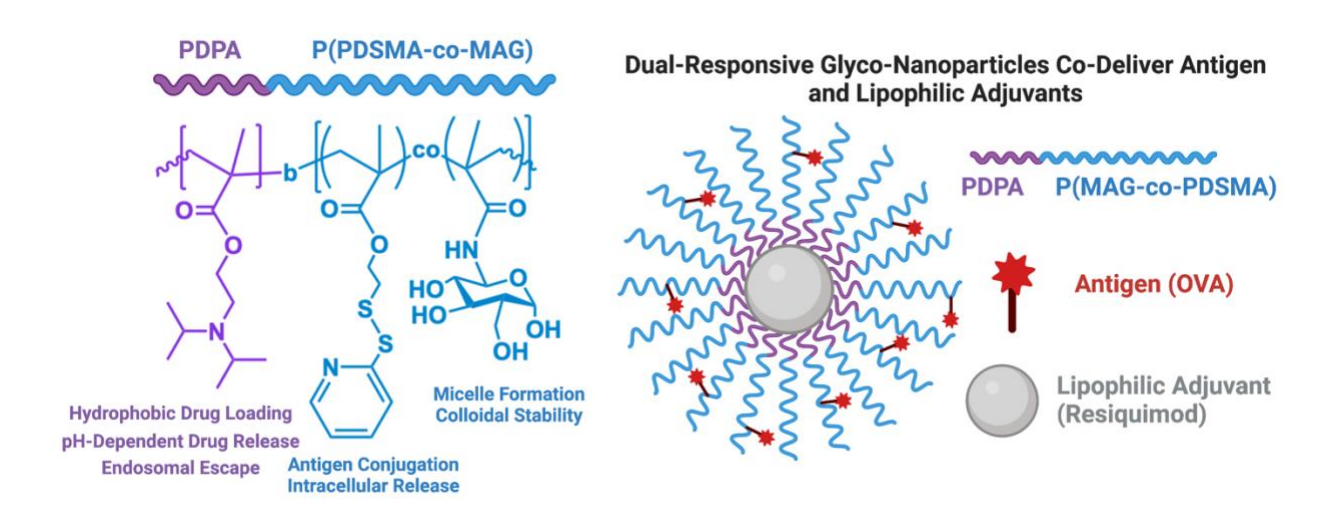
⁴Cancer Center and Research Institute, University of Mississippi Medical Center, Jackson, MS, USA, 39216

⁵Northwestern University Atomic and Nanoscale Characterization Experimental Center, Evanston, IL, USA, 60208

⁶Department of Chemical and Biomolecular Engineering, Vanderbilt University, Nashville, TN, USA, 37235

⁷Department of Chemistry, Louisiana State University, Baton Rouge, LA, USA, 70803

Table of Contents Graphic



Abstract

Traditional approaches to vaccines use whole organisms to trigger an immune response, but they do not typically generate robust cellular-mediated immunity and have various safety risks. Subunit vaccines composed of proteins and/or peptides represent an attractive and safe alternative to whole organism vaccines, but they are poorly immunogenic. Though there are biological reasons for the poor immunogenicity of proteins and peptides, one other key to their relative lack of immunogenicity could be attributed to the poor pharmacokinetic properties of exogenously delivered peptides. For instance, peptides often aggregate at the site of injection, are not stable in biological fluids, proteins are rapidly cleared from circulation, and both have poor cellular internalization and endosomal escape. Herein, we developed a delivery system to address the lack of protein immunogenicity by overcoming delivery barriers as well as codelivering immune-stimulating adjuvants. The glycopolymeric nanoparticles (glycoNPs) are composed of a dual stimuli-responsive block glycopolymer, poly[2-(diisopropylamino)ethyl methacrylate]-b-poly[(pyridyl disulfide ethyl methacrylate)-co-(methacrylamidoglucopyranose)] (p[DPA-b-(PDSMA-co-MAG)]). This polymer facilitates protein conjugation and cytosolic release, the pH-responsive release of lipophilic adjuvants, and pH-dependent membrane disruption to ensure cytosolic delivery of antigens. We synthesized p[DPA-b-(PDSMA-co-MAG)] by reversible addition-fragmentation chain transfer (RAFT) polymerization, followed by the formation and physicochemical characterization of glycoNPs using the p[DPA-b-(PDSMA-co-MAG)] building blocks. These glycoNPs conjugated the model antigen ovalbumin (OVA) and released OVA in response to elevated glutathione levels. Moreover, the glycoNPs displayed pHdependent drug release of the model hydrophobic drug Nile Red while also exhibiting pHresponsive endosomolytic behavior as indicated by a red blood cell hemolysis assay. GlycoNPs co-loaded with OVA and the toll-like receptor 7/8 (TLR-7/8) agonist Resiguimod (R848) activated DC 2.4 dendritic cells (DCs) significantly more than free OVA and R848 and led to robust antigen presentation of the OVA epitope SIINFEKL on major histocompatibility complex I (MHC-I). In sum,

the dual stimuli-responsive glycopolymer introduced here overcomes major protein and peptide delivery barriers and could vastly improve the immunogenicity of protein-based vaccines.

Keywords

Glycopolymer, subunit vaccine, immunotherapy, stimuli-responsiveness, Nanovaccine

Introduction

Subunit vaccines are an exciting molecular alternative to traditional vaccines composed of live-attenuated or deactivated whole pathogens because direct delivery of protein or peptide antigens enables precise molecular engineering of the immune response to vaccination.^{1,2} For instance, a precise antigen or combination of multiple antigens can be identified and delivered directly to induce antigen-specific responses. This approach has been validated for protein-based subunit vaccines as well as for neoantigen peptide vaccines for melanoma and other cancers.^{3,4} Additionally, whole pathogen-based vaccines pose safety risks due to potential virulence and the inclusion of unnecessary antigenic load and inflammatory pathogen-associated molecular patterns (PAMPs).⁵ Therefore, subunit vaccines could also significantly improve the safety of vaccines by preventing allergic reactions, auto-immune toxicities, or the risk of infection associated with whole pathogen vaccines. However, subunit vaccines composed of protein or peptide antigen are hampered by their relative lack of immunogenicity.

One key reason for the lack of immunogenicity of subunit vaccines is the abysmal pharmacokinetic properties of the protein and/or peptide antigens making up the vaccines. Proteins antigens that are soluble and absorbed into the circulation are not stable in biological fluids and are rapidly cleared from the circulation after injection.⁶ Proteins do not natively traffic well to lymph nodes and have very poor cell uptake, limiting their intake by antigen-presenting cells (APCs) which are needed to initiate a productive immune response.^{7,8} Additionally, the

endosomal escape of proteins is also limited, meaning that most of the therapeutic payload that reaches cells is degraded within the endolysosomal pathway.^{9,10} Additionally, many protein antigens inherently lack immunogenicity and require co-administration of potent adjuvants to boost the overall immune response.¹¹ Therefore, recent efforts have addressed the shortcomings of protein and peptide vaccine delivery using polymeric nanoparticles (NPs),^{12,13} liposomes/lipid-based particles,^{14,15} or conjugates.⁷ But the difficulty of concomitantly overcoming the diverse barriers that block efficient protein delivery continues to hamper the translation of engineered antigen-specific subunit vaccines.

Stimuli-responsive block copolymers are an attractive material for overcoming the barriers to protein and peptide delivery because of their tailorable properties, multi-functionality, and ability to deliver cargo in response to specific cellular and sub-cellular environmental cues. For instance, the pH-responsive polymer poly(propyl acrylic acid) (PPAA) has improved Ovalbumin (Ova) uptake, retention, and endosomal escape for vaccines and other applications. 10,16,17 Importantly, PPAA can deliver Ova into the cytosol, where it can then be processed for loading onto the major histocompatibility complex I (MHC I), which is a critical step for generating robust cytotoxic T cell (CTL/CD8+) responses. Jia et al. have developed pH-responsive micelles for different methods of intracellular drug delivery. In one instance, they produced unimolecular micelles of star-like copolymers with pH-sensitive linkage of Doxorubicin for pH-sensitive intracellular release. 18 In another instance, they produced unimolecular micelles composed of pH-responsive 2-(diisopropylamino) ethyl methacrylate for the combined intracellular delivery of Doxorubicin and a photothermal agent for chemo/photothermal cancer therapy. ¹⁹ To enable co-delivery of antigens with immune-stimulating adjuvants, Wilson et al. have utilized stimuli-responsive block copolymers composed of a combination of antigen/adjuvant complexing blocks and pHresponsive, endosomolytic blocks.²⁰ Their work has led cumulatively to the development of cationic NPs appropriate for local administration (*e.g.*, inhalation)²¹, PEGylated micelles²², and PEGylated polymersomes capable of cytosolic co-delivery of antigens and various adjuvants^{23,24}.

Here, we introduce a glycopolymeric NP (glycoNP) that is biocompatible, well under 100 nm in diameter, capable of protein complexation, reduction-triggered antigen release, and pH-triggered endosomolysis and adjuvant release. The system is composed of a dual stimuli-responsive glycopolymer, poly[2-(diisopropylamino)ethyl methacrylate]-b-poly[(pyridyl disulfide ethyl methacrylate)-co-(methacrylamidoglucopyranose)] (p[DPA-b-(PDSMA-co-MAG)]). PDPA forms the pH-responsive core of the glycoNP for loading of lipophilic adjuvants at neutral pH. PDPA also drives disassembly of the glycoNPs, drug release, and pH-dependent membrane disruption as it undergoes a hydrophilic phase transition within the acidic microenvironment of endosomal compartments. PDSMA facilitates the conjugation of protein antigens via disulfide bonds that can subsequently be reduced in the presence of elevated glutathione inside cells. MAG was chosen as an NP corona material because it provides outstanding colloidal stability, 25 conserves NP structure through lyophilization (as shown here), and can improve APC uptake compared to PEGylation. We demonstrate the synthesis, physicochemical characterization, stimuli responsiveness, and bioactivity of the glycoNPs, which we show can promote robust activation of dendritic cells (DCs) *in vitro*.

Materials and Methods

Materials. 2-(Diisopropylamino) ethyl methacrylate (DPA) (CAS 16715-83-6, code 730971, lot# MKCM8495), glucosamine HCl 99% crystalline (CAS 66-84-2, code G4875-25 g lot# BCCD2896), methacryloyl chloride (CAS 920-46-7, code 523216-100 mL lot# MKCJ5699), 2-iminothiolane hydrochloride (98% (TLC) powder), 5,5'-Dithiobis(2-nitrobenzoic acid) (Ellman's Reagent), 2,2'-Azobis(2-methylpropionitrile) (AlBN, 98%), reversible addition-fragmentation chain transfer

(RAFT) agent 4-cyano-4([(ethylsulfanyl)carbonothioyl]sulfanyl) pentanoic acid (ECT, CAS 1137725-46-2), Triethylamine (TEA, ≥ 99.5%), deuterium oxide (D₂O), chloroform-d (CDCl₃) dimethyl sulfoxide-d6 (DMSO-d6), and ovalbumin (> 98% powder) were purchased from Millipore Sigma. 2, 2'-dipyridyl disulfide (98%, Alfa Aesar), Nile Red (99%, Acros Organics), 2-Mercaptoethanol (98%, Fisher Chemical), Alexa Fluor® 488 (Thermo Fisher Scientific), and L-Cysteine HCl.H2O (> 99%, Thermoscientific) were purchased through Fisher Scientific. Mouse blood (BALB/C Mouse whole blood K2EDTA lot# MSE 397738) was generously provided by the Tanner Lab for hemolysis experiments. Resiquimod (R848) was purchased from Selleckchem (Cat.No. S8133, Lot #S813302, MW 314.38 g/mol, purity 99.8%) and was stored at -20 °C until use. Attune™ Focusing Fluid 1x and fluorescence-activated cell sorting (FACS) Buffer 1x were purchased from Thermo Fisher Scientific.

Homopolymerization of DPA and the formation of macromolecular chain transfer agent PDPA: DPA was first purified using a 50-200 μm alumina column to remove hydroquinone inhibitor. To a clean 100 mL round bottom flask equipped with a magnetic stir bar, inhibitor-free DPA (4.3 mL, 18.14 mmol), 0.02 g/mL AIBN in dioxane (0.1 mL, 0.0122 mmol), and ECT (52 mg, 0.197 mmol) were added with 30 mL of dioxane as the solvent. The mixture was then dissolved and purged under N₂ for 30 min at room temperature. The round bottom flask (sealed with a rubber septum) was then immersed in a pre-heated oil bath at 70 °C, stirring at 300 rpm overnight. Polymerization was stopped by cooling and exposure to air. The remaining dioxane was replaced with acetone, and the unreacted monomer was removed simultaneously by dialysis against acetone (dialysis tubing MWCO 1 kD). Acetone was subsequently removed by drying under vacuum to obtain purified poly[2-(diisopropylamino)ethyl methacrylate] (PDPA), a yellowish viscous material (1.62 g, 0.081 mmol). Proton nuclear magnetic resonance (¹H NMR) (400 MHz, CDCl₃, δ in ppm): 0.96-0.86 (-CH₂CCH₃, signal a), 1.14-0.97 (-NCH(CH₃)₂, signal b), 1.98-1.76 (-CH₂CH₂C(CH₃)(CN) and

 $-C\underline{H}_2C(CH_3)(CN)$, signal g and h), 2.19 ($-C\underline{H}_2C(CH_3)S$, signal f), 2.75-2.57 ($-NC\underline{H}_2CH_2$, signal d), 3.12-2.92 (s, $-NC\underline{H}(CH_3)_2$, signal c), 3.99-3.77 ($-OC\underline{H}_2CH_2$, signal e).

MAG synthesis: 2-methacrylamido glucopyranose (MAG) was synthesized using a previously published procedure²⁷. Briefly, D(+)-glucosamine hydrochloride (8.68 g, 40.25 mmol) was mixed with sodium carbonate (6.42 g, 60.57 mmol), sodium nitrate (0.175 g, 2.05 mmol), and 25 mL of DI water in a 100 mL round bottom flask equipped with a stir bar. The mixture was then cooled to -10 °C in an ice/salt bath. Then, methacryloyl chloride (3.9 mL, 39.92 mmol) was added dropwise with vigorous stirring (400 rpm). The solution temperature was maintained at 10 ± 2 °C during this time and for an additional 2 hr after mixing was completed. The mixture was then allowed to stir at 200 rpm for another 20 hr at room temperature. To a 500 mL round bottom flask, 200 mL of methanol was added, and the crude product was stirred into the solution for 15 min. The formed white precipitate was vacuum filtered and washed with methanol. Washings were combined, and the solvents were removed under vacuum until the remaining solution was ~100 mL. Next, the solution was absorbed into 30 g of silica gel, and the residual solvent was removed. The product was then purified by column chromatography using ethyl acetate/methanol 8:2 v/v as the mobile phase. The product (white crystalline) was recrystallized in a small amount of the same mobile phase and characterized by ¹H NMR in D₂O. ¹H NMR (400 MHz, D₂O, δ in ppm): 7.8 (s, 1H, signal j), 5.63 (s, 1H, signal h), 5.14 (s, 1H signal i), 5.16-5.15 (d, 1H, signal a), 4.73-4.70 (d, 1H, signal a), 3.91-3.37 (m, 6H, signal b,c,d,e and f), 1.87 (s, 3H, signal g).

PDSMA synthesis: Pyridyl disulfide ethyl methacrylate (PDSMA) monomer was prepared using the literature protocol^{28,29}. In brief 2, 2'-dipyridyl disulfide (DPDS) (10g, 45 mmol, 1eq) was dissolved in 100 mL of methanol and 1.2 mL of glacial acetic acid was added to it. To this mixture, a solution of mercaptoethanol (4.25 g, 54 mmol, 1.2eq) in 50 mL methanol was added dropwise

at room temperature with continuous stirring under inert atmosphere. The reaction mixture was stirred at room temperature overnight. The solvent was evaporated to get the crude product as a yellow oil which was purified by silica gel column chromatography using a mixture of ethyl acetate/hexane as eluent (10 to 40% EtOAc) to get the 2-(pyridin-2-yldisulfanyl) ethanol (PDSE) as a colorless oil (6g, 32mmol, yield 70%). ($R_f = 0.4$ in 40% EtOAc in Hexane).

To a solution of PDSE (5g, 27mmol, 1eq) in 50 mL of dry dichloromethane was added triethylamine (3.24 g, 32mmol, 1.2eq) under inert atmosphere and the mixture was cooled in an ice bath. To this cold mixture, a solution of methacryloyl chloride (2.8g, 27 mmol, 1eq) in 10 mL dichloromethane was added dropwise with continuous stirring. The reaction was monitored by thin-layer chromatography and stopped after consumption of alcohol, 8 h after stirring at room temperature. The reaction mixture was washed with distilled water (2 x 50mL) followed by brine 50 mL. The organic layer was dried over anhydrous Na_2SO_4 and concentrated to get the crude product as a yellow oil which was purified by silica gel column chromatography using a mixture of ethyl acetate/hexane as eluent (0 to 30% EtOAc) to get the desired product as light-yellow oil (5.15g, 20mmol, yield 76%). (R_f = 0.6 in 30% EtOAc in Hexane) 1H NMR: (CDCl₃, 400 MHz), δ (ppm): 8.5 (m, 1H), 7.7 (m, 1H), 7.6 (m, 1H), 7.1 (m, 1H), 6.1 (m, 1H), 5.6 (m, 1H), 4.4 (t, J = 6.4 Hz, 2H), 3.1 (t, J = 6.4 Hz, 2H), 1.9 (m, 3H).

P(DPA-b-P(MAG-co-PDSMA)) copolymerization: The PDPA macro-chain transfer agent (macroCTA) (200 mg, 0.01 mmol) was mixed with MAG (250 mg, 1.011 mmol), PDSMA (12 mg, 0.0469mmol), 0.10 mL AIBN in dimethylacetamide (DMAc; 3.28 mg/mL, 0.002 mmol), and 4.5 mL of the solvent (DMAc:EtOH 4:1 v/v) in a 10 mL round bottom flask. The reaction mixture was purged with N_2 for 30 min under continuous stirring to deoxygenate the solution. Subsequently, the polymerization was initiated in a 65 °C oil bath and allowed to react for 24 hours before cooling and exposure to air. Upon completion of the polymerization, the solution was added to a dialysis

tube (MWCO 1kD) and dialyzed against phosphate-buffered saline (PBS, pH 7.4) overnight. The solution was then freeze-dried to obtain p[DPA-b-(MAG-co-PDSMA)] as a white powder.

Polymer Characterization. 1H-NMR of PDPA homopolymer was prepared in deuterated chloroform (CDCl₃), and p[DPA-b-(MAG-co-PDSMA)] block copolymer was prepared in deuterated dimethyl sulfoxide (DMSO-d6) and recorded with a 400 MHz Bruker spectrometer. Fourier-transform infrared (FTIR) spectra were recorded with an Agilent Technologies Carry 600 Series FTIR Spectrometer in the attenuated total reflectance (ATR) mode with a diamond crystal, using a resolution of 4 cm⁻¹ and averaging 64 scans over a spectral range of 4000-400 cm⁻¹. The samples were characterized by Gel Permeation Chromatography with Multi Angle Light Scattering (GPC-MALS). All samples were dissolved overnight at a concentration of ~10 mg/mL. The separations were carried out using a Gastorr BG-34 degasser, an Agilent 1100 pump, and an Agilent 1100 autosampler. A guard column (10 µ, 50 x 7.8mm) and two Phenogel 300 x 7.8 mm columns (Phenomenex, Torrance, CA), connected in series: (1) 10µ, 10⁵Å (10K-1000K); (2) 10μ, MXM (100-10,000K) were used for the separation. For detection, a Wyatt Dawn EOS multiangle light scattering detector with a Helium-Neon laser (690 nm) and Waters 410 differential refractive index detector were used. All separations were done using an injection volume of 70 µL. Tetrahydrofuran (THF) (1mL/min) stabilized with 250 ppm of butylated hydroxytoluene (BHT) (1mL/min) was used as the solvent. Data acquisition and data processing were performed using the Astra 6 software (Wyatt). A dn/dc of 0.077 (mL/g) was used for the molecular weight calculations.

Nanoparticle (glycoNP) Formulation: Bare NPs (without protein conjugation or dye loading) were prepared by a thin film hydration method. Briefly, 20 mg of the freeze-dried polymer was mixed with 5 mL of methanol in a scintillation vial, and the solvent was evaporated under vacuum to create a thin film. The polymer film was then hydrated in PBS (pH 7.4) to obtain the desired

concentration (by placing the suspension in a shaker for >2 hrs). *In some occasions glycoNPs were formulated with i) Nile Red-loaded, ii) ovalbumin (OVA) conjugated iii) AlexaFluor labelled-OVA-conjugated iv) Resiquimod loaded v) Resquimod-loaded and OVA conjugated.* Nile Red-loaded glycoNPs were formed by combining 16 mg of the polymer with 0.3 μL of 0.05 mg/mL Nile Red in dichloromethane and 1.5 mL methanol in a scintillation vial and subsequently evaporating the organic solvents in a vacuum oven to obtain a thin film. To the dry thin film, 2 mL of Dulbecco's phosphate buffered saline (DPBS) buffer was added and allowed to mix in a shaker for >2 hrs to form dye-loaded glycoNPs. The resultant NP suspension was filtered through 0.2 μm polyvinylidene fluoride (PVDF) filters to remove un-encapsulated Nile Red before testing pH-dependent hydrophobic "drug" release. Fluorescent-OVA conjugated glycoNPs were prepared for NP uptake studies by conjugating thiolated Alexa Fluor® 488 labeled OVA. The conjugation procedure is described below. R848-loaded glycoNPs were formulated similarly by mixing 4.4 mL of 1 mg/mL polymer (4400 μg) in methanol and 320 μl of 1.375 μg/μl (440 μg) R848 in DMSO and drying the organic solvents to obtain a thin film and subsequently hydrating in buffers.

Protein Conjugation: OVA was conjugated to polymer chains through pyridil disulfide moieties of PDSMA following a procedure published previously²⁰. Briefly, OVA was thoiolated using 2-iminothiolane (Traut's reagent) and unincorporated 2-iminothiolane was removed using desalination columns. OVA:thiol ratio (~1:3) was determined by reacting with Ellman's reagent according to the manufacturer's instructions. Thiolated OVA was reacted with NPs (10:1 protein to polymer molar ratio) by mixing them in pH 8 PBS buffer. The conjugation reaction was observed by sodium dodecyl-sulfate polyacrylamide gel electrophoresis (SDS-PAGE).

Physicochemical Characterization of NPs: Dynamic light scattering (DLS) measurements, including hydrodynamic diameter and zeta-potential, were taken using a Malvern Zetasizer PRO on solutions prepared at 0.2 – 1.0 mg/mL and filtered through a 0.2 μm syringe filter. Cryogenic

transmission electron microscopy (cryo-TEM) samples were made by pipetting 4 µL of sample onto copper grids (200-mesh with a lacey carbon membrane, glow-discharged for 30 s in a PELCO easi Glow-discharger at 15 mA, with a chamber pressure of 0.24 mBar) and plunge-frozen into liquid ethane with an FEI Vitrobot Mark III cryo plunge freezing robot with 5 s blot time and blot offset of 0.5 mm. The grids were stored in liquid nitrogen until loaded into a Gatan 626.6 cryo transfer holder cooled down to -180 °C. Images were taken using a Hitachi HT7700 tungsten emission TEM at 120 kV and collected on a Gatan Orius 2K x 4.67K digital camera. Surface morphology of freeze-dried polymer, as well as freeze-dried glycoNP (OVA conjugated) powders, were obtained by field emission scanning electron microscopy (FESEM). The samples were mounted on 9 mm Al stubs using glued carbon tapes. The powders were sputter coated with gold (16 nm thickness) while supplied with argon gas during the process. Prepared samples were observed using a JEOL JSM-7200 FLV FE-SEM at an accelerating voltage of 15 kV (1 nm resolution).

pH-Dependent Drug Release: The pH-dependent drug release was demonstrated using Nile Red-loaded NPs (without protein conjugation). Three different phosphate buffers at pH 5.5, 6.5, and 7.4 (200 μL each) were mixed with equivalent amounts of the Nile Red-loaded NP suspension filtered through 0.2 μm PVDF filters to remove un-encapsulated Nile Red. The resultant solutions were transferred to a 96-well plate (triplicates) and the fluorescence intensity was measured over time using a BioTek Synery H1 plate reader at excitation and emission wavelengths of 530 nm and 635 nm, respectively. Time-dependent release data were normalized to the t=0 fluorescence (fluorescence intensity 100%) of glycoNPs in each buffer (pH 5.5, 6.5, 7.4).

Hemolysis: Red blood cells (RBCs) were obtained from BioIVT. After isolation, RBCs were incubated with varying concentrations (0 - 100 μg/mL total polymer concentration) of p[DPA-b-(MAG-co-PDSMA)] with and without OVA conjugation at three pH's representative of extracellular

and endolysosomal ranges (7.4, 6.5, 5.5). After 1 h of incubation, intact RBCs and cellular debris were centrifuged out, and supernatants were removed. The supernatants were measured for absorbance at 451 nm (hemoglobin absorbance) and percent hemolysis was determined relative to 1% Triton-X100 detergent.

Cell culture. DC 2.4 mouse dendritic cell line (Millipore Sigma) was cultured in Roswell Park Memorial Institute (RPMI) media (Millipore Sigma Cat. No. R6504) containing 10% fetal bovine serum (Gibco), 1X non-essential amino acids (Millipore Sigma Cat. No. TMS-001-0C), 1X HEPES buffer solution (Cat. No. TMS-003-C), 0.0054X β-mercaptoethanol (Millipore Sigma Cat. No. ES-007-E). RAW 264.7 mouse macrophage cell line (ATCC TIB-71) was purchased and cultured in Dulbecco's Modified Eagle's Medium (DMEM) media (Gibco) containing 10% FBS (Gibco) and 1% Anti-Anti reagent (Gibco). All cell lines were maintained at 37 °C and 5% CO₂.

Cell Viability. The cell viability of polymer treated RAW 264.7 murine macrophages was used to determine the cytocompatibility of the polymers. The cells in culture media were seeded in three replicates in a 96-well plate at a density of 5,000 cells/well. The cells were allowed to adhere and proliferate for 24 hr before replacing the media with new media containing varying concentrations of polymer solution (0-1000 µg/mL). The cells were incubated with the new media for 24 hr, after which the CellTiter Glo™ (Promega, Cat. No. G9242) assay was performed, and the luminescence of the cells was measured on a microplate reader (BioTek Synergy H1).

Cell Uptake. DC 2.4 cells were seeded in three replicates in 12-well plates at a density of 100,000 cells/well and allowed to adhere for 24 hr. Poly(2-methacrylamido glucopyranose) (PMAG) and poly(oligo ethylene glycol) methyl ether methacrylate (PEGMA) nanoparticles loaded with DiO were prepared at a concentration of 4 mg/mL. Before nanoparticle treatment, the quantity of DiO

encapsulated was adjusted to ensure both the PMAG and PEGMA nanoparticles had equivalent fluorescence intensity. Next, the nanoparticles were diluted with media to have a final concentration of 400 µg/mL. Next, the cells were treated with nanoparticle solution in media for 2 hr, washed with PBS and FACS buffer, fixed with formaldehyde, and kept in FACS buffer. Flow cytometric analysis was performed using an Invitrogen Attune NXT cytometer (ThermoFisher Scientific, Waltham, MA).

DC Cell Activation. To load R848 to NPs, a thin-film method was used. Polymer (4.4 mg) was dissolved in 1 mL of methanol and mixed with 320 μL of R848 stock solution (440 μg of R848). This maintained 10% R848 compared to polymer weight. The solutions were mixed well in a scintillation vial and dried under a vacuum to obtain a thin film. Simultaneously a thin film of the polymer was prepared (4.4 mg dissolved in 1 mL of methanol), and both were stored at 4°C (in the dark) until use. Polymer+R848 and polymer thin films were removed from 4°C and rehydrated with pH 8 PBS (2 mL) in the shaker for 2 hr. A 1 mL aliquot of freshly prepared thiolated OVA was added to the polymers with stirring.

Before treating cells with NPs, the particle solution was taken out of 4 °C and UV-vis absorbance at 328 nm was measured to quantify R848 and was used for serial dilution of free R848 stock solution to match the final amount of R848 used to treat cells (40 μg/mL). The final polymer concentration of R848 loaded NP solution (0.28 mg/mL) was used to calculate the serial dilution of the sample with bare NP treatment. The solutions were diluted 10 times (1:9) with RPMI media before addition to the DC 2.4 cells. DC 2.4 cells were cultured in a 12 well plate (500,000 cells/well) for 12 hours before the media was replaced with NP samples. After 12 hours, the cells were washed in PBS and FACS buffer and incubated with antibodies against either CD80 (eBioscienceTM, Cat. No. 12080182) or H-2Kb bound to SIINFEKL (BioLegend, Cat. No. 142606).

Statistics. Unless indicated otherwise, data are represented as average with a standard error of the mean (SEM). The Student's t-test was used to directly compare two treatment groups for statistical significance (p=0.05 threshold). One-way ANOVA was performed to assess statistical significance among three or more treatment populations, with Tukey's post-hoc test to determine the statistical difference between specific treatment groups (p=0.05 threshold).

Scheme 1. RAFT synthesis of p[DPA-*b***-(PDSMA-***co***-MAG)].** DPA is homopolymerized using ECT as a chain transfer agent to produce PDPA. Subsequently, PDSMA and MAG are copolymerized as a separate polymer block using PDPA as a macro-chain transfer agent.

Results

Synthesis of p[DPA-b-(PDSMA-co-MAG)] polymer. The dual-responsive, diblock glycopolymer, p[DPA-b-(PDSMA-co-MAG)], was produced by RAFT polymerization (**Scheme 1**). RAFT was utilized because it enables the generation of complex polymer architectures with precise control over the molecular weight and polydispersity of the resulting polymers. To enable

RAFT polymerization, MAG and PDSMA monomers were first generated. MAG was successfully produced by modifying D-(+)-glucosamine with methacryloyl chloride in a one-step reaction with high yield, as indicated by the presence of both methacrylate protons and alcohol protons in the ¹H-NMR spectrum (**Figure S1**). PDSMA monomer was generated by a two-step reaction where an alcohol was introduced to 2, 2'-dipyridyl disulfide followed by modification with methacryloyl chloride. ¹H-NMR also confirmed the successful synthesis and purification of PDSMA monomer (Figure S2). Next, we generated the PDPA block using ECT as the chain transfer agent (CTA) and confirmed the successful polymerization based on the appearance of the polymer backbone and side chain proton peaks in the ¹H-NMR spectra (Figure 1A). Using PDPA-ECT as a macroCTA, we synthesized the p(PDSMA-co-MAG) block. The resulting p(PDSMA-co-MAG) block was confirmed first based on the presence of protons associated with both PDSMA and MAG in the ¹H-NMR spectra (**Figure 1B**). To further confirm the successful polymerization of the diblock copolymer p[DPA-b-(PDSMA-co-MAG)], we conducted FTIR and observed the appearance of hydroxyl and amide peak stretching in the p[DPA-b-(PDSMA-co-MAG)] spectra as compared to PDPA (Figure 1C). Lastly, we conducted GPC analysis to determine the molecular weight and polydispersity of the PDPA homopolymer as well as the resulting p[DPA-b-(PDSMAco-MAG)] diblock copolymer. GPC results further confirmed the successful synthesis of p[DPAb-(PDSMA-co-MAG)] with a total molecular weight of 30 kDa and narrow polydispersity (1.09) (Figure 1D).

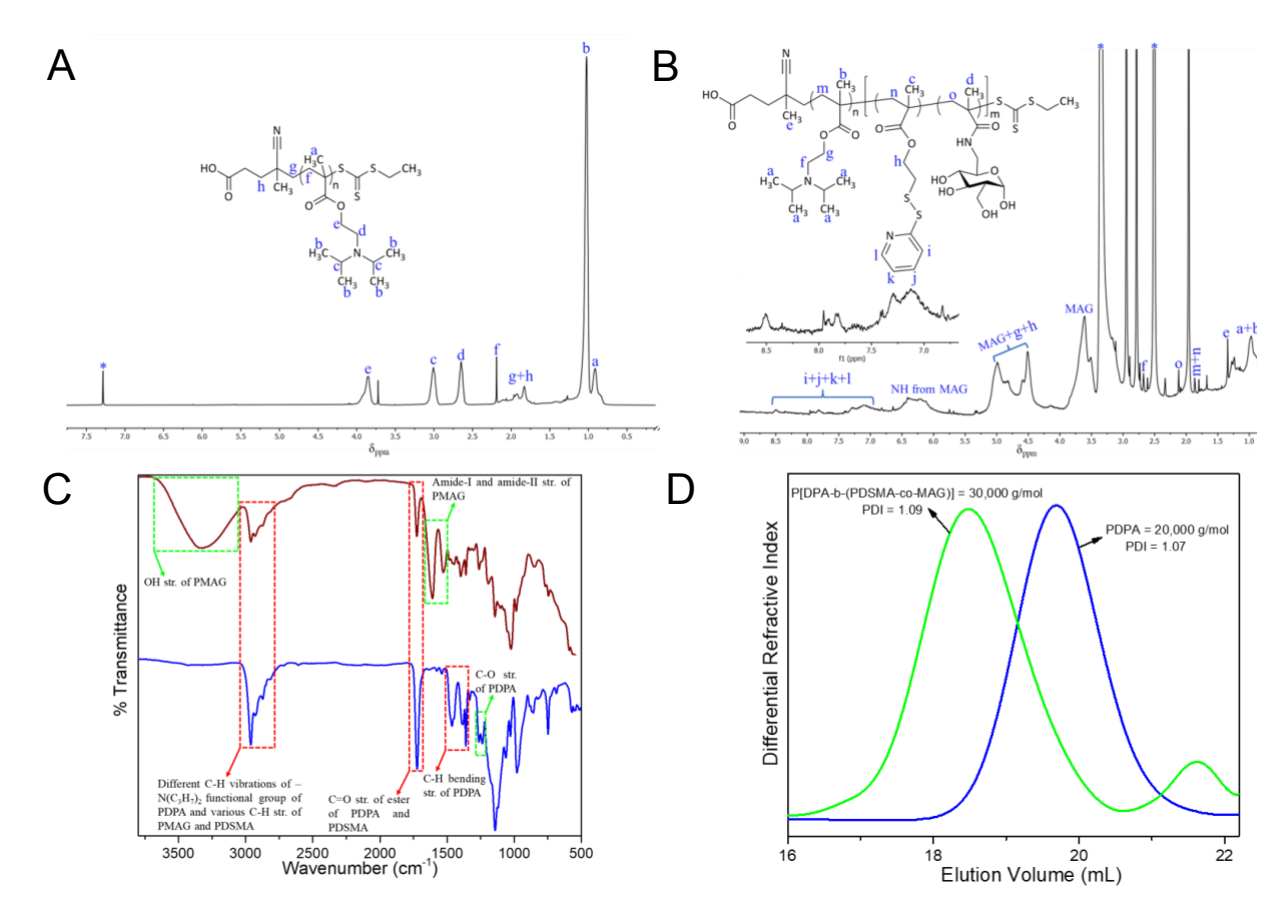


Figure 1. Chemical characterization of p[DPA-*b***-(PDSMA-***co***-MAG)]** . (a) ¹H NMR spectra of PDPA homopolymer in CDCl₃, (*) solvent peak, (b) p[DPA-*b*-(PDSMA-*co*-MAG)] block copolymer in DMSO-d6, (*) solvent peak, (c) ATR-IR spectra of PDPA homopolymer (bottom) and p[DPA-*b*-(PDSMA-*co*-MAG)] block copolymer (upper), and (d) GPC elugrams of PDPA homopolymer and p[DPA-*b*-(PDSMA-*co*-MAG)] block copolymer.

Physicochemical characterization of glyconanoparticles (glycoNPs). Upon preparation by a thin film hydration method, we characterized the size, morphology, and surface charge of the glycoNPs. We also used the glycoNPs to encapsulate lipophilic adjuvants and conjugate antigens, in this case, the model antigen OVA (Figure 2A). Cryo-TEM images suggested that glycoNPs form spherical aggregates under 100 nm in diameter (Figure 2B). This was consistent across multiple images and samples and is particularly exciting since it is well-established that particles in the range of 20-50 nm in diameter transport efficiently through tumors and accumulate well within lymph nodes. Dynamic light scattering (DLS) measurements further confirmed the cryo-TEM images, indicating that unloaded glycoNPs were ~30 nm in diameter, drug-loaded glycoNPs were ~40 nm in diameter, and protein-conjugated glycoNPs were ~60 nm in diameter (Table 1

and **Figure 2C**). Additionally, we determined that the glycoNPs had neutral (0.97 ± 0.1) to slightly positive $(9.06 \pm 0.95 \text{ mV})$ surface charge before and after protein conjugation, respectively (**Table 1** and **Figure 2D**).

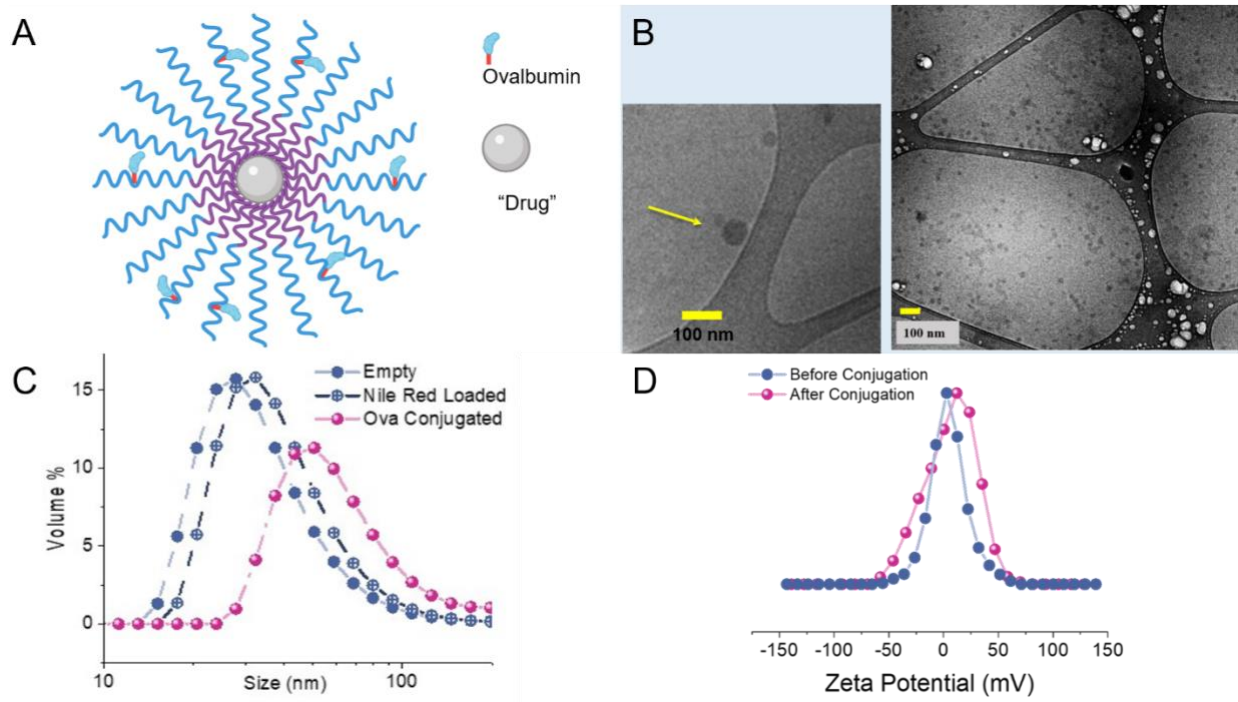


Figure 2. Physicochemical characterization of glycoNPs. (A) Schematic of glycoNPs; Micellar NPs are formed by the glycoNPs with antigen (e.g., OVA) attached to the corona, and lipophilic drugs (e.g., adjuvant) are coreloaded. **(B)** Cryo-TEM images of glycoNPs at high (left) and low (right) magnification. **(C)** DLS measurements of the hydrodynamic diameter of Empty, Nile Red Loaded, and OVA Conjugated glycoNPs. **(D)** Z-Potential (i.e., surface charge) distributions for glycoNPs before and after OVA conjugation.

Table 1. Nanoparticle Physicochemical Characteristics			
Sample	D _h (nm)	PD %	Zeta-Potential (mV)
Empty NPs	33.5 ± 0.4	37	0.97 ± 0.1 (before conjugation)
Nile Red-loaded NPs	38.8 ± 0.4	36	-
OVA-Conjugated	58.7 ± 1.5	34	9.06 ± 0.95 (after conjugation)
NPs			

Hydrodynamic diameters were obtained by log-normal fitting DLS distribution (volume fraction vs. size) data and the polydispersity percentages (PD%) were obtained by FWHM of the fits.³⁰ (\pm) represent standard error of the mean, n = 3. Dh = hydrodynamic diameter, PD% = polydispersity percentages.

Reversible Conjugation of Thiolated Antigen. We confirmed the ability of the glycoNPs designed here to reversibly conjugate protein antigen via a simple disulfide exchange with PDSMA using thiolated OVA as a model protein antigen (Figure 3A). Using SDS-PAGE, we observed the expected migration of OVA through the SDS-PAGE gel as indicated by the clear band appearing at ~45 kDa (*Lane v*; Figure 3B). Whereas a simple physical mixture of OVA (unthiolated) and polymer did not impact OVA migration in the gel (*Lane ii*), the migration of polymer-conjugated OVA was significantly disrupted, which is a strong indication of covalent conjugation to the polymer (*Lane iii*). Moreover, a portion of the OVA can be seen re-appearing at ~45 kDa upon the addition of glutathione (GSH) as a reducing agent (*Lane iv*), suggesting that the disulfide bond between OVA and the polymer backbone can be reduced for the release of OVA within reducing environments such as the cytosol of cells. Briefly, we also confirmed the cytocompatibility of OVA-conjugated and unconjugated polymers by observing no significant reduction in viability of a RAW 264.7 mouse macrophage cell line which was incubated overnight with increasing concentrations of polymer (Figure 3C).

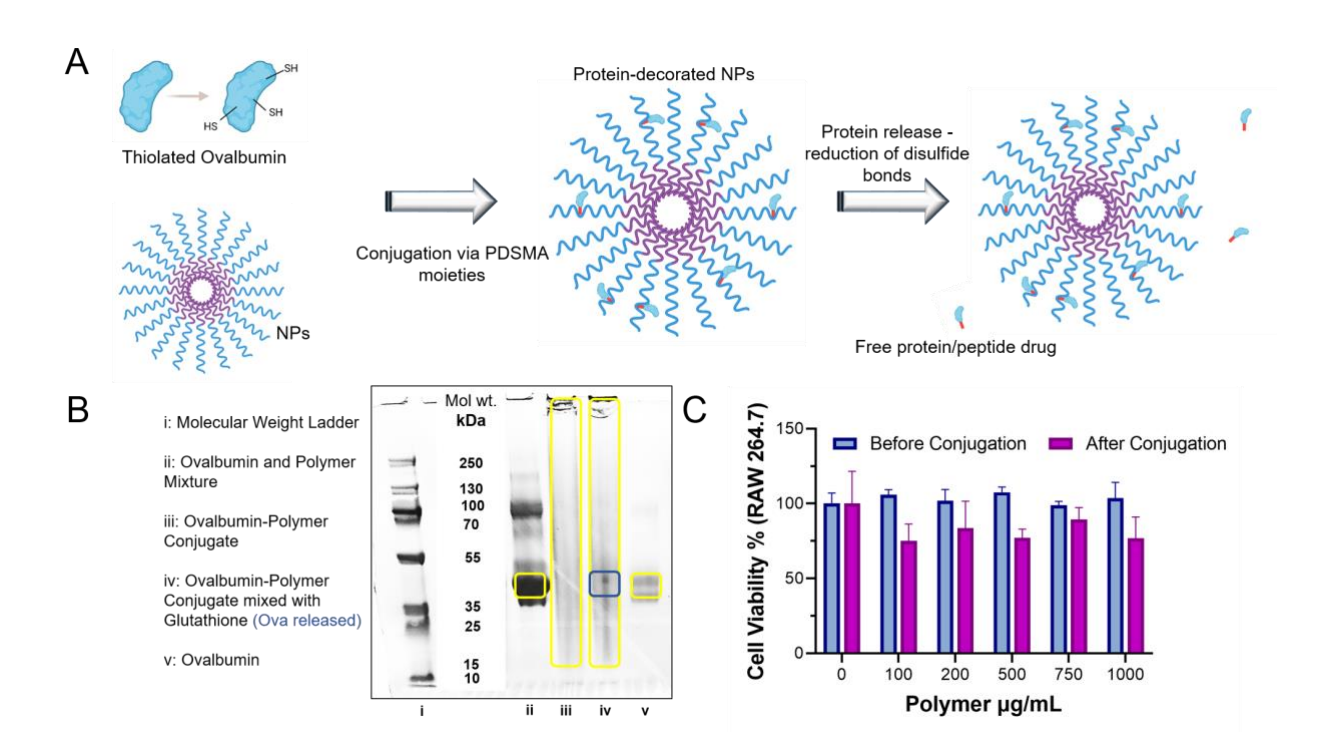


Figure 3. Conjugation of antigen to glycoNPs and biocompatibility before and after conjugation. (A) Schematic of conjugation of thiolated OVA to glycoNPs, followed by OVA release in reducing environments (e.g., cytosol). (B) SDS-PAGE gel to monitor OVA migration alone, OVA physically mixed with glycoNPs, OVA conjugated to glycoNPs, and OVA released from glycoNPs in the presence of glutathione. (C) Cell viability of glycoNPs before and after conjugation of OVA at $0-1,000~\mu g/mL$ glycoNP concentration.

PMAG conserves glycoNP structure through lyophilization. Sugars such as trehalose and various cyclodextrins have been shown to be effective excipients that preserve nanoparticle architecture through lyophilization and resuspension³¹⁻³³. Moreover, producing nano-vaccines that can survive the lyophilization process would be of great value since lyophilization would remove cold supply chain demands and allow for distribution and storage at ambient temperature. Therefore, we investigated whether the glycoNPs produced here could survive lyophilization since the surface of the NPs was composed of 95% sugar which is similar in structure and property to many common excipients. Scanning electron microscopy (SEM) images show the microscopic structure of lyophilized p[DPA-*b*-(PDSMA-*co*-MAG)] polymer before glycoNP formation (Figure 4A and S3; bottom left). Next, glycoNPs were prepared from thin films, dispersed in an aqueous solution, frozen, and then lyophilized. Upon re-examination by SEM, the lyophilized glycoNPs formed interconnected sheets that were distinct in structure from the original polymeric powder (Figure 4A and S3; top right). Cryo-TEM images confirmed that, upon resuspension in PBS, the lyophilized glycoNPs formed spherical particles with the same size and distribution as freshly-prepared glycoNPs in PBS (Figure 4B).

pH-Dependent Drug Release and Lipid Bilayer Disruption. Next, we investigated the pH-responsiveness of the glycoNPs with two distinct goals in mind. First, we designed the glycoNPs to achieve drug release specifically in acidic pHs found within the endolysosomal pathway. That way, it would be possible to deliver high doses of adjuvant to pattern recognition receptors (PRRs) such as toll-like receptors (TLRs) that reside within endosomes. To test the ability of glycoNPs to achieve this pH-dependent drug release, we loaded glycoNPs with Nile Red (which loses its fluorescence when released from micelles) and monitored the fluorescence of Nile Red-loaded glycoNPs at pH 7.4, 6.5, and 5.5. Although only negligible reduction in Nile Red fluorescence is

observed over 12 hrs at pH 7.4, the fluorescence of the Nile Red-loaded glycoNPs is rapidly lost at pHs 6.5 and 5.5 (**Figure 5A**). Moreover, the loss in Nile Red fluorescence is pH-dependent, where a more rapid and complete reduction of Nile Red fluorescence was observed at pH 5.5 compared to pH 6.5.

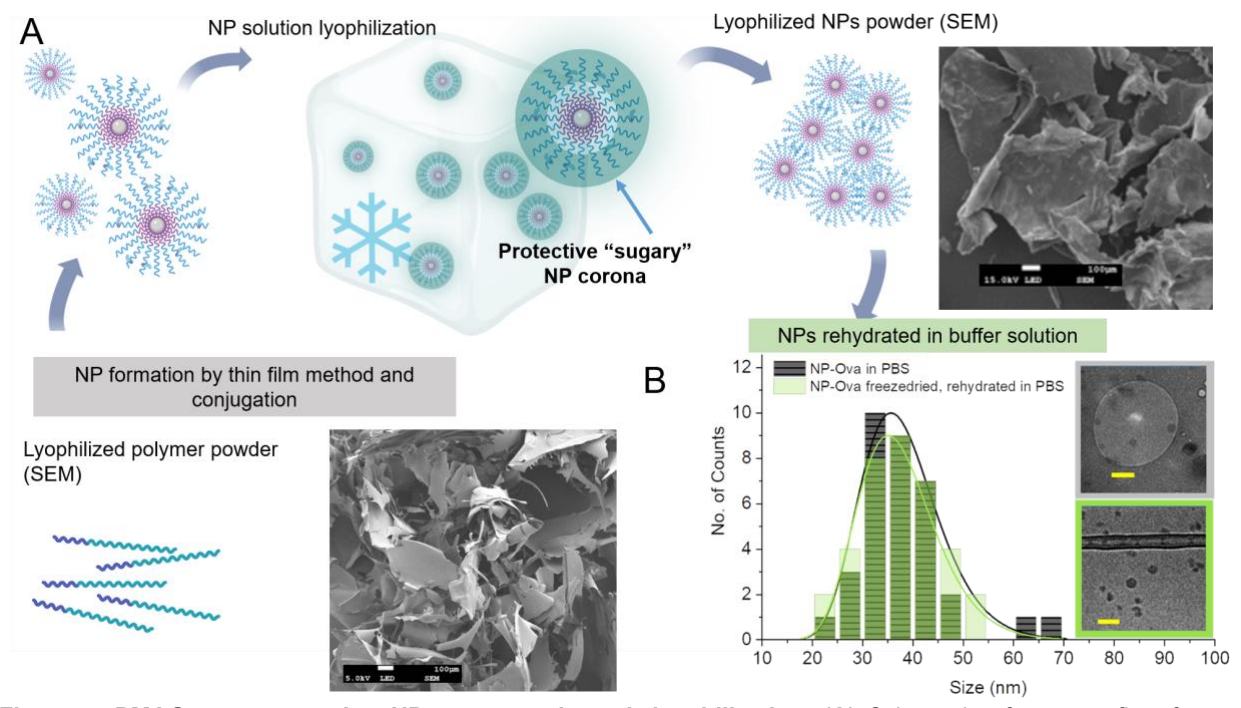


Figure 4. PMAG conserves glycoNP structure through lyophilization. (A) Schematic of process flow from lyophilized polymer to NP formation and lyophilization followed by rehydration in buffer solution. SEM images show representative samples of lyophilized polymer powder (bottom left) and lyophilized glycoNPs (top right). **(B)** Histograms and representative Cryo-EM images (yellow scale bars = 100nm) of freshly-prepared glycoNPs and rehydrated glycoNPs.

The second design objective for the pH-responsive behavior of the glycoNPs was to achieve pH-dependent lipid membrane disruption. Specifically, our goal was to engineer the glycoNPs to be inert to membranes at neutral pH (7.4) to maintain cytocompatibility but to selectively permeabilize membranes at acidic pHs indicative of the endolysosomal pathway (5.5 and 6.5). This would allow for the endosomal escape of antigen and delivery into the cytosol, resulting in the loading and presentation of antigen on MHC-I, which is vital for generating a robust CD8+ cytotoxic T cell (CTL) response (**Figure 5B**). Indeed, both the "naked" polymer and OVA-

conjugated polymers displayed robust, pH-dependent membrane disruption when incubated with red blood cells at pH 8, 7.4, 6.5, and 5.5 (**Figure 5C-D**). Specifically, the polymers were completely inert to red blood cell membranes at neutral pH and above (pH 8 or 7.4), whereas polymers lysed membranes at pH 6.5 and 5.5 in both a dose-dependent and pH-dependent manner. Importantly, OVA conjugation to the polymer did not appear to cause any significant reduction in membrane lysis by the polymers at acidic pH, indicating that the glycoNPs can effectively lyse membranes in the presence of conjugated antigen, which could then be shuttled into the cytosol for MHC-I processing.

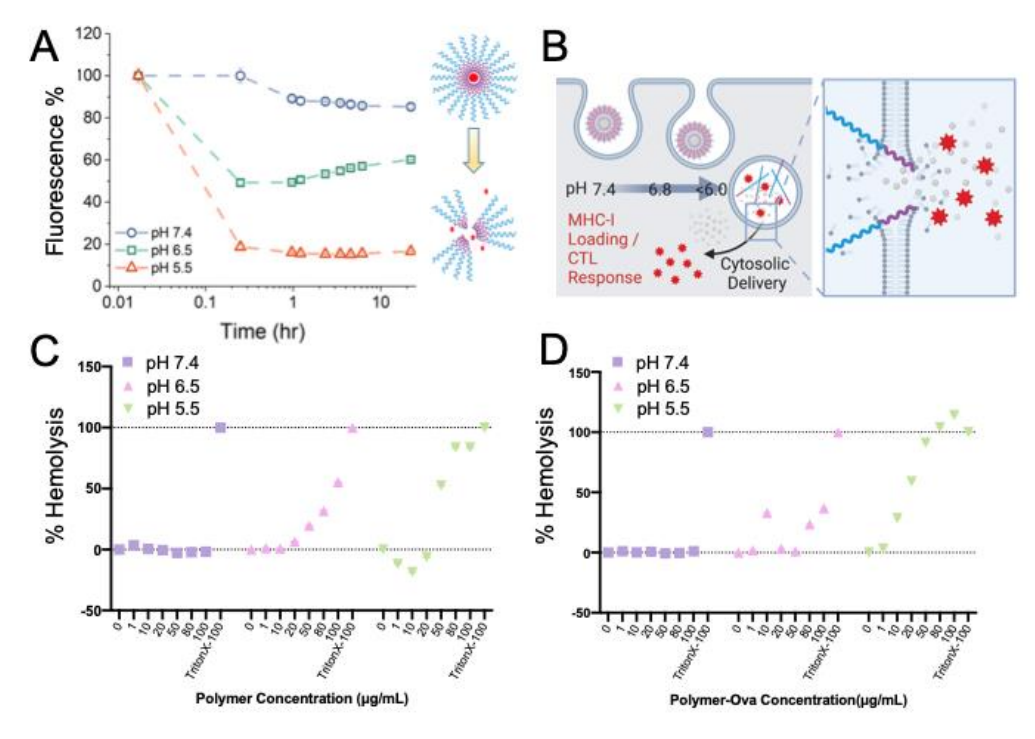


Figure 5. pH-responsive behavior of glycoNPs. (A) Release kinetics of Nile Red from glycoNPs at pH 7.4, 6.5, and 5.5. **(B)** Schematic of pH-dependent glycoNP dissasembly and lipid membrane disruption. %Hemolysis of red blood cell membranes at pHs 7.4, 6.5, and 5.5 for glycoNPs **(C)** before OVA conjugation and **(D)** after OVA conjugation.

Uptake of GlycoNPs in Antigen Presenting Cells. Since others have recently employed glycoconjugated antigens for improved APC targeting^{34,35}, we were interested to see if the glycoNPs developed here improved uptake in APCs compared to an analogous PEGylated NP. Therefore,

we compared the uptake of p[DPA-b-PEGMA] (PEGMA NPs; **Figure S4-5**) and p[DPA-b-MAG] (PMAG NPs) in DC 2.4 dendritic cells *in vitro*. After 2 hrs incubation, PMAG NPs displayed ~166x increased uptake compared to no treatment and PEGMA NPs – which displayed limited uptake above background levels (**Figure 6A**). These results highlight the ability of PMAG NPs to significantly increase uptake in APCs, and importantly to provide much higher doses of antigen and adjuvant cargo to the targeted APCs.

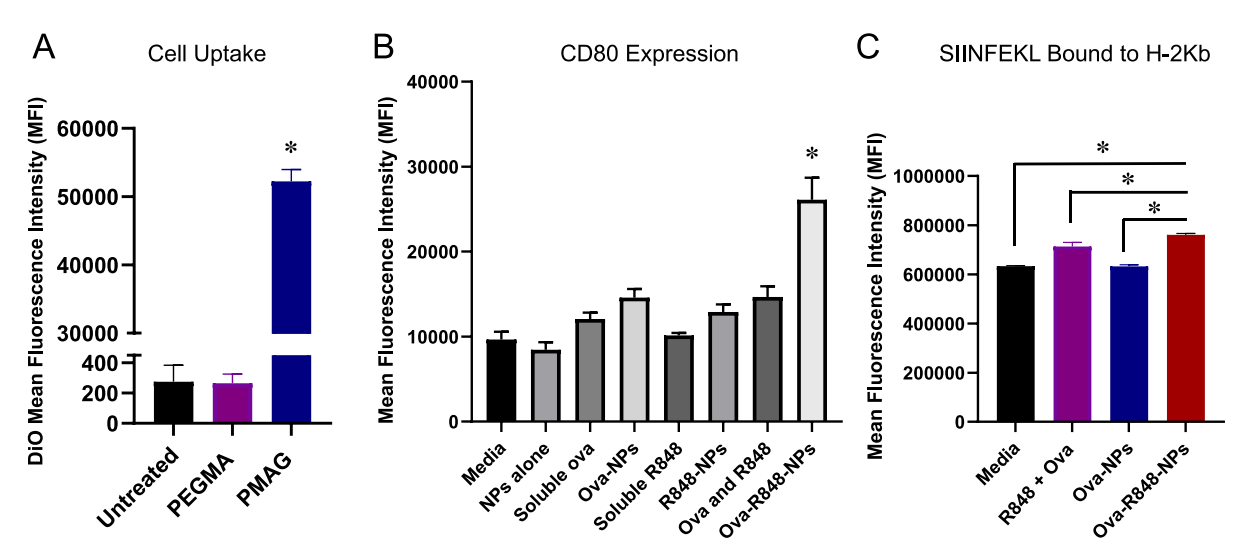


Figure 6. GlycoNPs improve activation of dendritic cells *in vitro.* **(A)** Cell uptake of DiO-loaded PEGMA NPs and PMAG NPs in DC 2.4 cells. **(B)** CD80 expression in DC 2.4 cells. **(C)** SIINFEKL bound to H-2Kb in DC 2.4 cells that were treated with R848 and OVA or OVA-NPs. Statistically significant difference (p-value < 0.05) is indicated by (*), n = 4.

Activation of Dendritic Cells *In Vitro*. Having confirmed the potential of glycoNPs to achieve high uptake and endosomal escape in APCs, we lastly wanted to investigate whether the glycoNPs could improve DC activation and antigen-presentation *in vitro* compared to the delivery of soluble antigen and adjuvants. Therefore, we generated glycoNPs loaded with the TLR 7/8 agonist R848 and conjugated to OVA as a model antigen. Subsequently, we treated DC 2.4 cells in culture with media, soluble OVA, soluble R848, OVA and R848, NPs alone, OVA-NPs, R848-NPs, and OVA-R848-NPs, and monitored DC 2.4 activation via induction of CD80 on flow

cytometry. Although NPs alone had no impact on CD80 expression, OVA-R848-NPs significantly increased CD80 expression to ~2.5x above untreated levels and ~2x above treatment with soluble R848 and OVA (Figure 6B). In all cases, NPs improved the induction of CD80 (i.e., OVA-NP vs. OVA, R848-NP vs. R848, and OVA-R848-NPs vs. OVA and R848). However, OVA-R848-NPs were the only treatment group that significantly increased CD80 expression above untreated controls, highlighting the value of glycoNP-based co-delivery of antigen and adjuvant for improving antigen immunogenicity. Lastly, we analyzed the expression of SIINFEKL bound to H-2Kb of MHC-I to assess whether the glycoNPs produced here could improve antigen presentation on MHC-I as hypothesized. Although OVA NPs (NPs carrying OVA alone) did not significantly improve MHC-I antigen presentation compared to untreated cells, OVA-R848-NPs induced a statistically significant increase in the presence of SIINFEKL antigen on MHC-I (Figure 6C). Moreover, R848 increased the presentation of SIINFEKL antigen whether it was encapsulated in NPs or not, but NP co-encapsulation of R848 with conjugated OVA resulted in improved antigen presentation compared to co-delivery of soluble R848. These results further highlight the importance of the glycoNP design since co-delivery of antigen and adjuvant were necessary to achieve improvements in both DC activation and antigen presentation.

Discussion

We developed and validated *in vitro* a dual stimuli-responsive glycoNP for the intracellular co-delivery of protein antigens and lipophilic immune adjuvants. These multifunctional glycoNPs are rationally designed to overcome the comprehensive delivery barriers faced by subunit vaccines. Protein antigens are reversibly conjugated to the glycoNPs to ensure solubilization, prevent precipitation upon injection, and protect the antigens from rapid clearance. The glycoNPs facilitate the uptake of antigen into APCs such as dendritic cells and facilitate co-delivery of antigen and adjuvant within a single, sub-100 nm diameter particle. The glycoNPs incorporate a

pH-responsive switch for the endosomal escape of antigens and drug release within cells, as well as a reduction-sensitive antigen linkage to facilitate cytosolic release.

Glycopolymers have recently emerged as exciting biomimetic drug delivery systems. Maynard et al. developed a number of synthetic techniques to produce proteins modified with trehalose-based polymers, which have been very effective at stabilizing proteins through lyophilization, improving shelf-life, bioactivity, and pharmacokinetic properties^{31,32}. Reineke et al. developed trehalose-coated cationic polyplexes to deliver nucleic acids, including short interfering RNA (siRNA) and plasmid DNA (pDNA)33,36,37. In this context, trehalose provides improved colloidal stability to the polyplexes compared to PEGylated analogs. Moreover, Reineke et al. have seen similar results with nucleic acid polyplexes coated with glucose-based polymers such as PMAG investigated in this study, where PMAG enhances polyplex stability compared to PEGylated analogs^{25,38}. Recently, mannosylated polymers have been under heavy investigation due to their ability to target M2-polarized macrophages that characteristically overexpress CD206/MMR³⁹⁻⁴². In addition, mannose polymer-drug conjugates can effectively target biofilms⁴³, and antigens conjugated to mannosylated polymers are taken up more efficiently by APCs, generating potent cellular and humoral immune responses³⁵. One reason we focused on glucosylated polymers instead of mannosylated polymers is because of their relative ease of synthesis. Compared to low yield, 3- or 4-step protocols to produce site-specific methacrylate moieties onto mannose sugars for RAFT polymerization, MAG can be produced in a one-step, one-pot reaction from D-(+)-glucosamine with greater than 95% yield²⁷. Importantly, the resulting glucosylated polymers can also efficiently target APCs as we have shown here, so there may be little trade-off in substituting the difficult and inefficiently synthesized mannosylated polymers for glucosylated analogs.

Compared to PEGylation, PMAG offers a variety of potential benefits as an NP surface engineering moiety. Two important considerations have been brought to light by the development and distribution of the COVID-19 mRNA nano-vaccines: 1) allergic reactions to PEG⁴⁴ and 2) cold

supply chain demands⁴⁵. PMAG has the potential to circumvent allergic reactions documented in response to PEGylated nano-vaccines.⁴⁴ PMAG also enables the lyophilization and resuspension of glycoNPs, which could prevent the need for cold supply chains as long as the biologically active cargo remain bioactive through the lyophilization process.^{31-33,36,45} Additionally, although we did not compare directly here, Reineke et al. demonstrated improved stability of NPs coated in PMAG compared to PEG³⁸. PMAG also enables active targeting of macrophages,²⁶ and as shown for the first time in these studies, dendritic cells. Thus, we believe that PMAG is an exciting surface engineering approach that is particularly well-suited to immunoengineering applications since it circumvents allergies to PEG, preserves NP architecture though lyophilization, and naturally targets NPs to APCs.

Subunit vaccines for infectious and emergent diseases are limited by their inability to produce robust cellular and humoral immune responses. The immunogenicity of these vaccines lags behind that of traditional, whole organism vaccines because of the loss of antigens and native adjuvants such as PAMPs on the microorganisms. The multifunctional glycoNPs developed here have the potential to overcome these shortcomings by improving the cytosolic delivery of antigens for loading onto MHC-I, as well as enabling co-delivery of adjuvants that can significantly boost immune stimulation in response to antigen/adjuvant co-delivery. Neoantigen cancer vaccines are particularly attractive applications for the glycoNPs developed here since the CD8+ T cell responses that are critical for anti-tumor immunity necessitate cytosolic delivery of peptide antigens. Moreover, it is now clear that the success of neoantigen cancer vaccines will necessitate the co-delivery of many tumor antigens jointly. Therefore, glycoNPs that can solubilize and deliver diverse neoantigens would be a valuable tool to prevent antigen aggregation at injection sites. Further investigations are needed to confirm the in vivo trafficking and immune stimulation of the glycoNPs introduced here, but the current studies provide support for the potential of dual stimuliresponsive glycoNPs to improve the delivery, and therefore efficacy, of protein-based subunit vaccines.

Conclusions

Future vaccination efforts will be aided by the ability to precisely engineer immune responses by the direct delivery of immunogenic protein and peptide antigens. We have developed a delivery system that overcomes the myriad of barriers that hamper protein delivery to the immune system. The p[DPA-b-(PDSMA-co-MAG)] glycoNPs introduced here effectively co-deliver protein antigens and lipophilic immune adjuvants. The dual stimuli-responsive nature of the glycoNPs ensures precise subcellular delivery of the vaccine components, where R848 is released within endosomes to engage TLRs, and antigens are released within the cytosol for MHC-I loading and antigen presentation. Co-delivery of the model antigen OVA and R848 induced robust activation of DCs and antigen presentation of the SIINFEKL epitope of OVA *in vitro*. Notably, the glycopolymer PMAG provides protection of the glycoNPs through lyophilization and facilitates their targeting of APCs - distinct advantages when compared to analogous PEGylated NPs. In sum, the glycoNPs developed here represent a multifunctional stimuli-responsive delivery system with the potential to improve the immune response to protein antigens and protein antigen/adjuvant combinations.

Acknowledgements

Research reported in this publication was supported by an Institutional Development Award (IDeA) from the National Institute of General Medical Sciences of the National Institutes of Health under award number P20GM103460. This material is based upon work supported by the National Science Foundation under Grant CAREER 2141666. The authors would also like to thank the University of Mississippi's Glycoscience Center of Research Excellence (GlyCORE) Analytical, Computation, and Imaging Research Cores for experimental consultation and support. This work made use of the BioCryo facility of Northwestern University's NUANCE Center, which has

received support from the SHyNE Resource (NSF ECCS-2025633), the International Institute for Nanotechnology (IIN), and Northwestern's MRSEC program (NSF DMR-1720139).

Supporting Information

Additional experimental details, materials, and methods, as well as additional characterization data, including ¹H NMR spectra and EM images for the materials used in the reported studies.

References

- 1. Malonis RJ, Lai JR, Vergnolle O. Peptide-Based Vaccines: Current Progress and Future Challenges. *Chem Rev.* Mar 25 2020;120(6):3210-3229. doi:10.1021/acs.chemrev.9b00472
- 2. Skwarczynski M, Toth I. Peptide-based synthetic vaccines. *Chem Sci.* Feb 1 2016;7(2):842-854. doi:10.1039/c5sc03892h
- 3. Ott PA, Hu Z, Keskin DB, et al. An immunogenic personal neoantigen vaccine for patients with melanoma. *Nature*. Jul 13 2017;547(7662):217-221. doi:10.1038/nature22991
- 4. Hacohen N, Fritsch EF, Carter TA, Lander ES, Wu CJ. Getting personal with neoantigen-based therapeutic cancer vaccines. *Cancer Immunol Res.* Jul 2013;1(1):11-5. doi:10.1158/2326-6066.CIR-13-0022
- 5. Karch CP, Burkhard P. Vaccine technologies: From whole organisms to rationally designed protein assemblies. *Biochem Pharmacol*. Nov 15 2016;120:1-14. doi:10.1016/j.bcp.2016.05.001
- 6. Diao L, Meibohm B. Pharmacokinetics and pharmacokinetic-pharmacodynamic correlations of therapeutic peptides. *Clin Pharmacokinet*. Oct 2013;52(10):855-68. doi:10.1007/s40262-013-0079-0
- 7. Liu H, Moynihan KD, Zheng Y, et al. Structure-based programming of lymph-node targeting in molecular vaccines. *Nature*. Mar 27 2014;507(7493):519-22. doi:10.1038/nature12978
- 8. Mehta NK, Moynihan KD, Irvine DJ. Engineering New Approaches to Cancer Vaccines. *Cancer Immunol Res.* Aug 2015;3(8):836-43. doi:10.1158/2326-6066.CIR-15-0112

- 9. Li H, E. Nelson C, C. Evans B, L. Duvall C. Delivery of Intracellular-Acting Biologics in Pro-Apoptotic Therapies. *Current Pharmaceutical Design*. // 2011;17(3):293-319. doi:10.2174/138161211795049642
- 10. Evans BC, Hocking KM, Kilchrist KV, Wise ES, Brophy CM, Duvall CL. Endosomolytic Nano-Polyplex Platform Technology for Cytosolic Peptide Delivery To Inhibit Pathological Vasoconstriction. *ACS Nano*. Jun 23 2015;9(6):5893-907. doi:10.1021/acsnano.5b00491
- 11. Meng J, Zhang P, Chen Q, et al. Two-Pronged Intracellular Co-Delivery of Antigen and Adjuvant for Synergistic Cancer Immunotherapy. *Adv Mater*. May 2022;34(21):e2202168. doi:10.1002/adma.202202168
- 12. Ilyinskii PO, Roy CJ, O'Neil CP, et al. Adjuvant-carrying synthetic vaccine particles augment the immune response to encapsulated antigen and exhibit strong local immune activation without inducing systemic cytokine release. *Vaccine*. May 19 2014;32(24):2882-95. doi:10.1016/j.vaccine.2014.02.027
- 13. Scott EA, Stano A, Gillard M, Maio-Liu AC, Swartz MA, Hubbell JA. Dendritic cell activation and T cell priming with adjuvant- and antigen-loaded oxidation-sensitive polymersomes. *Biomaterials*. Sep 2012;33(26):6211-9. doi:10.1016/j.biomaterials.2012.04.060
- 14. Kuai R, Ochyl LJ, Bahjat KS, Schwendeman A, Moon JJ. Designer vaccine nanodiscs for personalized cancer immunotherapy. *Nat Mater*. Apr 2017;16(4):489-496. doi:10.1038/nmat4822
- 15. Hanson MC, Abraham W, Crespo MP, et al. Liposomal vaccines incorporating molecular adjuvants and intrastructural T-cell help promote the immunogenicity of HIV membrane-proximal external region peptides. *Vaccine*. Feb 11 2015;33(7):861-8. doi:10.1016/j.vaccine.2014.12.045
- 16. Qiu F, Becker KW, Knight FC, et al. Poly (propylacrylic acid)-peptide nanoplexes as a platform for enhancing the immunogenicity of neoantigen cancer vaccines. *Biomaterials*. 2018;182:82-91.
- 17. Foster S, Duvall CL, Crownover EF, Hoffman AS, Stayton PS. Intracellular delivery of a protein antigen with an endosomal-releasing polymer enhances CD8 T-cell production and prophylactic vaccine efficacy. *Bioconjug Chem.* Dec 15 2010;21(12):2205-12. doi:10.1021/bc100204m
- 18. Jia T, Huang S, Yang C, Wang M. Unimolecular Micelles of Amphiphilic Cyclodextrin-Core Star-Like Copolymers with Covalent pH-Responsive Linkage of Anticancer Prodrugs. *Molecular Pharmaceutics*. 2017/08/07 2017;14(8):2529-2537. doi:10.1021/acs.molpharmaceut.6b00708
- 19. Jia T, Huang S, Yang C, Wang M. Unimolecular micelles of pH-responsive star-like copolymers for co-delivery of anticancer drugs and small-molecular photothermal agents: a new drug-carrier for combinational chemo/photothermal cancer therapy. 10.1039/C7TB01657C. *Journal of Materials Chemistry B*. 2017;5(43):8514-8524. doi:10.1039/C7TB01657C

- 20. Wilson JT, Keller S, Manganiello MJ, et al. pH-Responsive nanoparticle vaccines for dual-delivery of antigens and immunostimulatory oligonucleotides. *ACS Nano*. May 28 2013;7(5):3912-25. doi:10.1021/nn305466z
- 21. Knight FC, Gilchuk P, Kumar A, et al. Mucosal Immunization with a pH-Responsive Nanoparticle Vaccine Induces Protective CD8(+) Lung-Resident Memory T Cells. *ACS Nano*. Oct 22 2019;13(10):10939-10960. doi:10.1021/acsnano.9b00326
- 22. Carson CS, Becker KW, Garland KM, et al. A nanovaccine for enhancing cellular immunity via cytosolic co-delivery of antigen and polyIC RNA. *Journal of controlled release : official journal of the Controlled Release Society*. May 2022;345:354-370. doi:10.1016/j.jconrel.2022.03.020
- 23. Shae D, Becker KW, Christov P, et al. Endosomolytic polymersomes increase the activity of cyclic dinucleotide STING agonists to enhance cancer immunotherapy. *Nat Nanotechnol*. Mar 2019;14(3):269-278. doi:10.1038/s41565-018-0342-5
- 24. Shae D, Baljon JJ, Wehbe M, et al. Co-delivery of Peptide Neoantigens and Stimulator of Interferon Genes Agonists Enhances Response to Cancer Vaccines. *ACS Nano*. Aug 25 2020;14(8):9904-9916. doi:10.1021/acsnano.0c02765
- 25. Wu Y, Wang M, Sprouse D, Smith AE, Reineke TM. Glucose-Containing Diblock Polycations Exhibit Molecular Weight, Charge, and Cell-Type Dependence for pDNA Delivery. research-article. *Biomacromolecules*. April 25, 2014 2014;doi:10.1021/bm5001229
- 26. Shofolawe-Bakare OT, de Mel JU, Mishra SK, et al. ROS-Responsive Glycopolymeric Nanoparticles for Enhanced Drug Delivery to Macrophages. *Macromol Biosci*. Sep 20 2022:e2200281. doi:10.1002/mabi.202200281
- 27. Pearson S, Allen N, Stenzel MH. Core-shell particles with glycopolymer shell and polynucleoside core via RAFT: From micelles to rods. https://doi.org/10.1002/pola.23275. Journal of Polymer Science Part A: Polymer Chemistry. 2009/03/15 2009;47(6):1706-1723. doi:https://doi.org/10.1002/pola.23275
- 28. Iamsaard S, Seidi F, Dararatana N, Crespy D. Redox-responsive polymer with self-immolative linkers for the release of payloads. *Macromolecular Rapid Communications*. 2018;39(12):n/a.
- 29. Ghosh S, Basu S, Thayumanavan S. Simultaneous and Reversible Functionalization of Copolymers for Biological Applications. *Macromolecules*. 2006;39(17):5595-5597.
- 30. De Mel JU, Gupta S, Willner L, et al. Manipulating Phospholipid Vesicles at the Nanoscale: A Transformation from Unilamellar to Multilamellar by an n-Alkyl-poly(ethylene oxide). *Langmuir*. 2021/02/23 2021;37(7):2362-2375. doi:10.1021/acs.langmuir.0c03302

- 31. Mancini RJ, Lee J, Maynard HD. Trehalose glycopolymers for stabilization of protein conjugates to environmental stressors. *J Am Chem Soc.* May 2012;134(20):8474-9. doi:10.1021/ja2120234
- 32. Lee J, Lin EW, Lau UY, Hedrick JL, Bat E, Maynard HD. Trehalose glycopolymers as excipients for protein stabilization. *Biomacromolecules*. Aug 2013;14(8):2561-9. doi:10.1021/bm4003046
- 33. Srinivasachari S, Liu Y, Zhang G, Prevette L, Reineke TM. Trehalose click polymers inhibit nanoparticle aggregation and promote pDNA delivery in serum. *J Am Chem Soc.* Jun 2006;128(25):8176-84. doi:10.1021/ja0585580
- 34. Tokatlian T, Read BJ, Jones CA, et al. Innate immune recognition of glycans targets HIV nanoparticle immunogens to germinal centers. *Science*. Feb 8 2019;363(6427):649-654. doi:10.1126/science.aat9120
- 35. Wilson DS, Hirosue S, Raczy MM, et al. Antigens reversibly conjugated to a polymeric glyco-adjuvant induce protective humoral and cellular immunity. *Nat Mater*. Feb 2019;18(2):175-185. doi:10.1038/s41563-018-0256-5
- 36. Srinivasachari S, Liu Y, Prevette LE, Reineke TM. Effects of trehalose click polymer length on pDNA complex stability and delivery efficacy. *Biomaterials*. Jun 2007;28(18):2885-98. doi:10.1016/j.biomaterials.2007.01.037
- 37. Sizovs A, Xue L, Tolstyka ZP, et al. Poly(trehalose): sugar-coated nanocomplexes promote stabilization and effective polyplex-mediated siRNA delivery. *J Am Chem Soc.* Oct 2013;135(41):15417-24. doi:10.1021/ja404941p
- 38. Smith AE, Sizovs A, Grandinetti G, Xue L, Reineke TM. Diblock Glycopolymers Promote Colloidal Stability of Polyplexes and Effective pDNA and siRNA Delivery under Physiological Salt and Serum Conditions. research-article. *Biomacromolecules*. July 15, 2011 2011;doi:10.1021/bm200643c
- 39. Song EH, Manganiello MJ, Chow YH, et al. In vivo targeting of alveolar macrophages via RAFT-based glycopolymers. *Biomaterials*. Oct 2012;33(28):6889-97. doi:10.1016/j.biomaterials.2012.06.025
- 40. Yu SS, Lau CM, Barham WJ, et al. Macrophage-Specific RNA Interference Targeting via "Click", Mannosylated Polymeric Micelles. research-article. *Molecular Pharmaceutics*. February 12, 2013 2013;doi:10.1021/mp300434e
- 41. Ortega RA, Barham WJ, Kumar B, et al. Biocompatible mannosylated endosomal-escape nanoparticles enhance selective delivery of short nucleotide sequences to tumor associated macrophages. *Nanoscale*. Jan 2015;7(2):500-10. doi:10.1039/c4nr03962a

- 42. Su FY, Srinivasan S, Lee B, et al. Macrophage-targeted drugamers with enzyme-cleavable linkers deliver high intracellular drug dosing and sustained drug pharmacokinetics against alveolar pulmonary infections. *Journal of controlled release : official journal of the Controlled Release Society.* Oct 10 2018;287:1-11. doi:10.1016/j.jconrel.2018.08.014
- 43. Limqueco E, Passos Da Silva D, Reichhardt C, et al. Mannose Conjugated Polymer Targeting P. aeruginosa Biofilms. *ACS Infect Dis.* Nov 13 2020;6(11):2866-2871. doi:10.1021/acsinfecdis.0c00407
- 44. McSweeney MD, Mohan M, Commins SP, Lai SK. Anaphylaxis to Pfizer/BioNTech mRNA COVID-19 Vaccine in a Patient With Clinically Confirmed PEG Allergy. *Front Allergy*. 2021;2:715844. doi:10.3389/falgy.2021.715844
- 45. Fahrni ML, Ismail IA, Refi DM, et al. Management of COVID-19 vaccines cold chain logistics: a scoping review. *J Pharm Policy Pract*. Mar 2 2022;15(1):16. doi:10.1186/s40545-022-00411-5